Separation of Quaternary Conjugate Salt Systems by Fractional Crystallization

David A. Berry and Ka M. Ng
Dept. of Chemical Engineering, University of Massachusetts, Amherst, MA 01003

A method is presented that synthesizes fractional crystallization separation processes to obtain pure solids from conjugate salt solutions. The method, which includes a procedure to generate phase diagrams by using solubility products, explains how to calculate concentrations of all components in a system given a point on a Jänecke projection. Both multivalent ions and species that exhibit complex-ionic equilibrium are considered. For solutions from which only simple salts crystallize, three separation classes are identified. The classification is based on the composition of the feed, the characteristics of the phase diagram, and the product salts. Class I separates compatible salts, Class II incompatible salts, and Class III two compatible salts and one incompatible salt. Process paths and design equations for each class are also presented. Guidelines proposed select the separation sequence and the stream compositions based on the effects of the design variables on stream flows and on total annual cost. The method is applicable to systems in which hydrates and double salts are present. An example given shows how to obtain simple salts from these systems.

Introduction

Fractional crystallization effects separations by manipulating the relative solubilities of the components in a solution by dilution, evaporation, dissolution, stream combination, and temperature swing. The technique is used to separate a wide variety of chemicals. For example, minerals such as borax, lithium sulfate monohydrate, potash, sodium carbonate, and sodium chloride are crystallized from brines (Hightower, 1951; Mehta, 1988; Jongema, 1993). Sodium tripolyphosphate is precipitated from solutions of soda ash and orthophosphoric acid (Ainsworth, 1994). Of equal importance is the fractional crystallization of organic salts to resolve optically active fine chemicals and pharmaceuticals (Paul and Rosas, 1990; Stinson, 1994). For example, one of the steps in the manufacture of both cilastatin and permethrin is to crystallize an optically pure diastereoisomeric salt that is a precursor to the final product (Fogassy et al., 1988; Meul, 1992).

Despite the significance of fractional crystallization of salts, little information is available on the conceptual design of these processes. Purdon and Slater (1946) gave a detailed account of the use of temperature and solvent swings to effect crystallization. An abbreviated version is found in Mullin (1993). Fitch (1970) discussed various fractional crystallization schemes. Cisternas and Rudd (1993) extended this work. A limitation of all the designs just listed is that they are based on points of multiple saturation where cocrystallization occurs. Also, calculation of phase diagrams and solubilities is not addressed. And the effects of incomplete dissociation and complex-ionic equilibrium on design equations are not considered.

Recently, systematic methods have been developed for the conceptual design of crystallization processes for molecular systems. Rajagopal et al. (1991) and Dye and Ng (1995a) discussed the use of extractive crystallization to completely separate two and three solutes from a solution, respectively. A similar approach was taken for the conceptual design of fractional crystallization processes (Rajagopal et al., 1988; Dye and Ng, 1995b). Furthermore, Ng (1991) provided a systematic method to separate a multicomponent mixture of molecular solids.

This article gives a design method to synthesize fractional crystallization processes for separating conjugate salts from systems composed of simple and compound salts. The objective is to identify process alternatives, constraints, and costs. First, we discuss the generation of phase diagrams. The exploitable features of a phase diagram essential for synthesizing separation schemes are identified. The calculations nec-

Correspondence concerning this article should be addressed to K. M. Ng.

essary to solve for the concentration of any component in the system given a point on a Jänecke projection are presented. Second, we propose three general separation classes to obtain pure salts. The process paths, equipment configurations, and design equations are given for each class. Based on the effects of the design variables on the flows and on the total annual cost, guidelines are proposed for the selection of the separation sequence and the compositions of the streams. Third, we show that the operations used in systems of simple salts, can be used to recover pure salts from systems containing compounds and hydrates.

Description of Phase Behavior

A quaternary conjugate salt system is formed by dissolving two salts without a common ion in an inert solvent. As a result of a metathesis reaction, a total of four simple salts may precipitate from solution. For example, consider the reaction between salts A_xX_a and B_yY_b to produce A_yY_a and B_xX_b:

$$\frac{1}{ax}A_xX_a+\frac{1}{by}B_yY_b=\frac{1}{ay}A_yY_a+\frac{1}{bx}B_xX_b, \qquad (1)$$

where A_xX_a and B_yY_b are conjugate salts of A_yY_a and B_xX_b. The ions of the salts may incompletely dissociate, interact via complex-ionic equilibrium, or they may also react to form compounds (Butler, 1964; Fleck, 1966). The conditions under which specific salts precipitate are represented on a phase diagram.

Figure 1 is a phase diagram for an aqueous system formed from monovalent salts in Eq. 1, where A^+, B^+, X^- and Y^- represent $\Delta-[Co(ox)(en)_2]^+$, $\Lambda-[Co(ox)(en)_2]^+$, Cl^-, and d-H_3tart^-, respectively. The coordinates of a point on the diagram are given by the ratio of $[B]$ to the total cation concentration (r_B), by the ratio of $[Y]$ to the total anion concentration (r_Y), and by the mass of solvent per equivalent of salt ($1/z$). Points labeled with *AX*, *BY*, *AY*, and *BX* are solutions of the respective pure salt dissolved in solvent. The *double-saturation points* (*K*, *L*, *M*, and *N*) represent solutions saturated with the two salts along the same edge of the diagram. The *triple-saturation points* (*P* and *Q*) are saturated with three salts (*AX*, *BY*, *BX*, and *AX*, *BY*, *AY*, respectively). The regions bounded by *AX-L-Q-P-K*, *BY-N-P-Q-M*, *AY-L-Q-M*, and *BX-K-P-N* represent the *saturation surfaces* for *AX*, *BY*, *AY*, and *BX*, respectively. These surfaces represent the conditions where a pure salt is equilibrated with solution. The system is saturated with two salts along the *double-saturation troughs PK*, *PN*, *PQ*, *QL*, and *QM*. *AX* and *BY* are called *compatible salts* because these salts contain all the ions in the system and they coexist along trough *PQ*. Conversely, *AY* and *BX* are the *incompatible salts*.

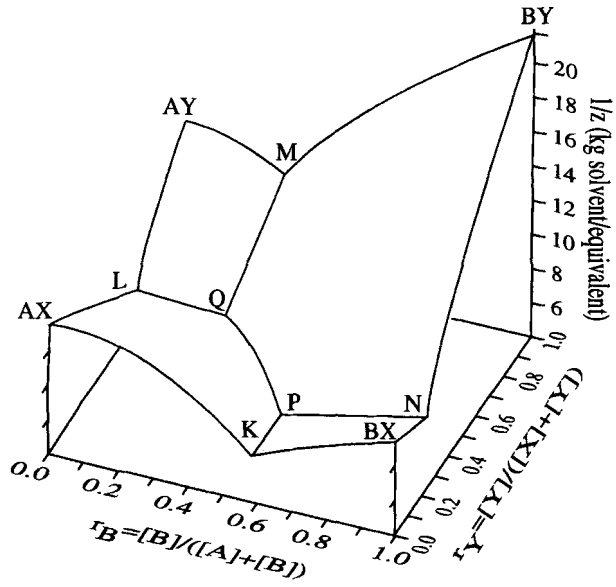

Figure 1. Phase diagram for a conjugate salt pair of optically active cobalt(III) complexes at 25°C.

AX = Δ-$[Co(ox)(en)_2]Cl$, *AY* = Δ-$[Co(ox)(en)_2]$*d*-H_3tart, *BX* = Λ-$[Co(ox)(en)_2]Cl$, and *BY* = Λ-$[Co(ox)(en)_2]$*d*-H_3tart.

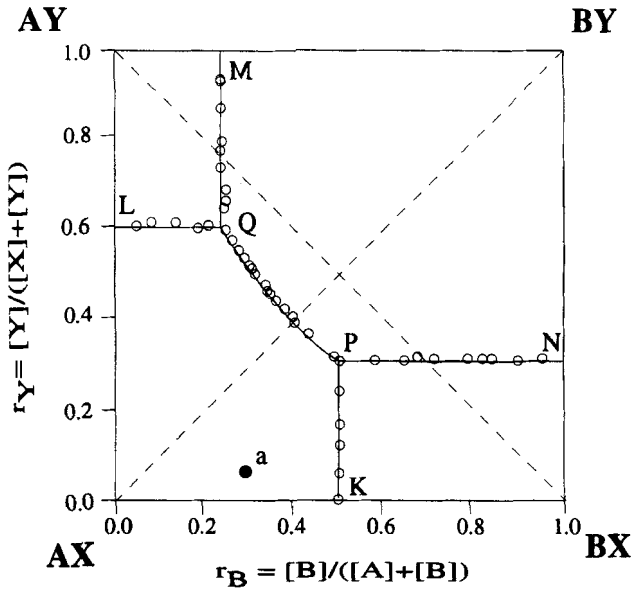

Figure 2. Jänecke projection for (Λ-$[Co(ox)(en)_2]^+$, Δ-$[Co(ox)(en)_2]^+$)-(Cl^-, $d-H_3tart^-$) at 25°C.

The salts are represented by the notation given in Figure 1. The solubility products of the salts are $K_{AX}=4\times10^{-3}$, $K_{AY}=4\times10^{-3}$, $K_{BX}=6\times10^{-3}$, and $K_{BY}=8\times10^{-3}$. Open circles are experimental data due to Fuyuhiro (1979).

Figure 2 is the Jänecke projection of the same system. The diagonal joining the (in)compatible salts is called the *(in)compatible salt-pair diagonal.* The surfaces, troughs, and points on the projection are labeled in an identical fashion as in the square-prism phase diagram. Both diagram and projection were calculated by using solubility products. The calculations required to generate a phase diagram and Jänecke projection will be discussed in the following section. Furthermore, even though the system was assumed to be an ideal solution, the model results are in good agreement with experimental data (open circles) due to Fuyuhiro et al. (1979).

Although a quaternary system has a maximum of six degrees of freedom, a maximum of three solid phases may coexist on phase diagrams used for design of crystallization processes. The phase diagram is insensitive to pressure because

the system is condensed. One degree of freedom is taken by specifying the existence of a solution phase at all compositions. Another degree of freedom is taken by specifying the temperature. One should note that there is an invariant point at which four solids equilibrate with solution. Therefore, it is possible for the compatibility of the salt pairs to be reversed by a change of temperature. For example, in the aqueous system $NaIO_3 \cdot H_2O + KCl = NaCl + KIO_3 + H_2O$, the first pair is compatible below, the second pair above 39.5°C (Ricci, 1951). In most systems, the conditions at which compatibility inversion occurs are not appropriate for crystallization processes; therefore, we do not consider this phenomenon in the sections that follow.

Calculation of Jänecke projections by using solubility products

Solubility products are used to generate Jänecke projections of quaternary conjugate salt solutions. Values for solubility products of sparingly soluble salts at 298 K can be found in Chang (1990), Sohnel and Garside (1992), among others. The values of the solubility products may either increase or decrease with temperature. The method to calculate the Jänecke projections does not change.

In this section it is assumed that compounds do not form and that the salts completely dissociate in the solvent. The ordinate (r_B) and the abscissa (r_Y) of the Jänecke projection are given by

$$r_B = \frac{[B]/b}{[A]/a + [B]/b} \tag{2}$$

$$r_Y = \frac{[Y]/y}{[X]/x + [Y]/y} \tag{3}$$

To calculate the coordinates of point P, use the following solubility products:

$$K_{A_xX_a} = (\gamma_{A_xX_a})^{(a+x)/ax}[A]^{1/a}[X]^{1/x} \tag{4}$$

$$K_{B_xX_b} = (\gamma_{B_xX_b})^{(b+x)/bx}[B]^{1/b}[X]^{1/x} \tag{5}$$

$$K_{B_yY_b} = (\gamma_{B_yY_b})^{(b+y)/by}[B]^{1/b}[Y]^{1/y} \tag{6}$$

The solubility products are on a one-equivalent basis to avoid raising the activity coefficients and ionic concentrations to large exponents (Meissner and Kusik, 1979). Models for calculating the activity coefficient are given elsewhere (Pitzer, 1973; Nicolaisen et al., 1993). After rearranging Eqs. 4 through 6, the following ratios can be calculated for given values of the solubility products:

$$R_B = \frac{[B]^{1/b}}{[A]^{1/a} + [B]^{1/b}} = \frac{(\gamma_{A_xX_a})^{(a+x)/ax}K_{B_xX_b}}{(\gamma_{B_xX_b})^{(b+x)/bx}K_{A_xX_a} + (\gamma_{A_xX_a})^{(a+x)/ax}K_{B_xX_b}} \tag{7}$$

$$R_Y = \frac{[Y]^{1/y}}{[X]^{1/x} + [Y]^{1/y}} = \frac{(\gamma_{B_xX_b})^{(b+x)/bx}K_{B_yY_b}}{(\gamma_{B_yY_b})^{(b+y)/by}K_{B_xX_b} + (\gamma_{B_xX_b})^{(b+x)/bx}K_{B_yY_b}}. \tag{8}$$

In order to plot point P in the coordinate system used in Jänecke projections (Figure 2), it is necessary to transform R_B to r_B and R_Y to r_Y. Because an analytical transformation is not possible, the following procedure is given to obtain the relationship between r_B and R_B. By assuming values for $[A]$ and $[B]$, the values of r_B and R_B are calculated using Eqs. 2 and 7, respectively. This procedure is repeated for the entire range of r_B and R_B between 0.0 and 1.0. Figure 3 shows r_B as a function of R_B for the specific case of $a = 2$ and $b = 3$. A similar relationship between r_Y and R_Y can be determined by assuming values for $[X]$ and $[Y]$. The coordinates of the other triple-saturation point Q are calculated in a similar manner; however, in this case the solubility products for B_yY_b, A_xX_a, and A_yY_a are used in the calculations.

The double-saturation troughs PK, PN, QL, QM, and PQ are calculated from the solubility products of the two salts that equilibrate along the respective trough. For example, consider the compatible-salt trough, PQ. By multiplying R_B and R_Y one obtains

$$R_BR_Y = \frac{K_{B_yY_b}}{\gamma_{B_yY_b}^{(b+y)/by}([A]^{1/a} + [B]^{1/b})([X]^{1/x} + [Y]^{1/y})}. \tag{9}$$

Multiplying $(1 - R_B)$ and $(1 - R_Y)$ gives

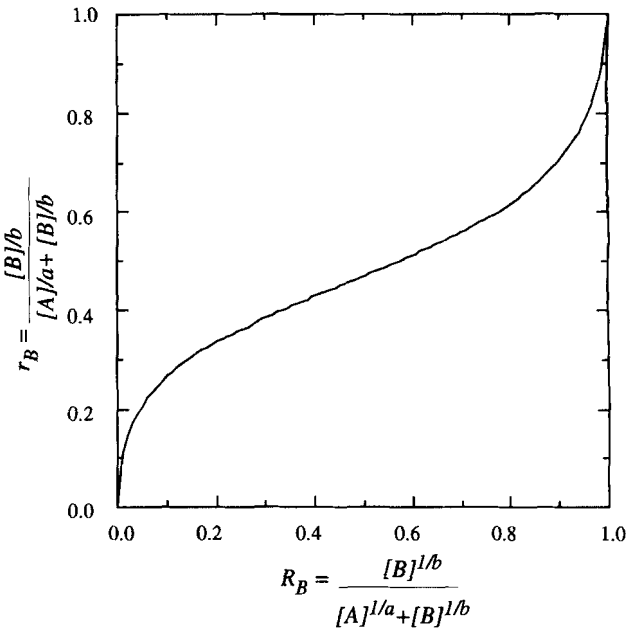

Figure 3. Relationship between r_B and R_B for $a = 2$ and $b = 3$.

$$(1-R_B)(1-R_Y) = \frac{K_{A_xX_a}}{\gamma_{A_xX_a}^{(a+x)/ax}([A]^{1/a}+[B]^{1/b})([X]^{1/x}+[Y]^{1/y})}. \quad (10)$$

Solving for R_B using Eqs. 9 and 10 gives

$$R_B = \frac{(1-R_Y)\gamma_{A_xX_a}^{(a+x)/ax}K_{B_yY_b}}{R_Y\left(K_{A_xX_a}\gamma_{B_yY_b}^{(b+y)/by} - \gamma_{A_xX_a}^{(a+x)/ax}K_{B_yY_b}\right) + \gamma_{A_xX_a}^{(a+x)/ax}K_{B_yY_b}}. \quad (11)$$

R_Y is obtained from Eq. 9. The values of R_B and R_Y are transformed to r_B and r_Y, respectively, by use of a plot such as the one given in Figure 3. The compatible-salt trough is generated by plotting several values of r_B and r_Y onto the Jänecke projection. It can be shown that PQ is always a curve. In contrast, the other double-saturation troughs are straight lines perpendicular to their respective edges in Figure 2. These troughs only become curved as a result of complex-ionic equilibrium or nonideality.

Calculation of salt solubilities and concentrations

From the coordinates of a point plotted on a Jänecke projection, it is possible to calculate the concentrations of all the species in the solution. To illustrate the required calculations, consider point ***a*** on Figure 2. A charge balance gives

$$z = a[A]+b[B] = x[X]+y[Y]. \quad (12)$$

The mass of solvent per equivalent is given by $1/z$. Eliminating $[B]$ in Eq. 12 with Eq. 2, we get

$$[A] = \frac{a(1-r_B)z}{a^2+(b^2-a^2)r_B}. \quad (13)$$

Similarly, we get from Eqs. 12 and 3

$$[X] = \frac{x(1-r_Y)z}{x^2+(y^2-x^2)r_Y}. \quad (14)$$

Since point ***a*** lies on the A_xX_a saturation surface, this is the only solubility product used in these calculations. Substituting $[A]$ and $[X]$ from Eqs. 13 and 14 into Eq. 4 and then solving for z gives

$$z = \frac{(K_{A_xX_a})^{ax/(a+x)}}{\gamma_{A_xX_a}}\left\{\frac{a^2+(b^2-a^2)r_B}{a(1-r_B)}\right\}^{x/(a+x)} \times\left\{\frac{x^2+(y^2-x^2)r_Y}{x(1-r_Y)}\right\}^{a/(a+x)}. \quad (15)$$

By using Eqs. 13 through 15, the concentrations $[A]$ and $[X]$ can be calculated. The concentrations of $[B]$ and $[Y]$ are

$$[B] = \frac{br_Bz}{a^2+(b^2-a^2)r_B} \quad (16)$$

$$[Y] = \frac{yr_Yz}{x^2+(y^2-x^2)r_Y}. \quad (17)$$

The concentrations calculated in Eqs. 13 through 17 can be used to calculate the solubility and concentrations of the salts as follows:

$$S_{A_xX_a} = \begin{cases} W_{A_xX_a}[A]/x \text{ if } [A]/x < [X]/a \\ W_{A_xX_a}[X]/a \text{ if } [X]/a < [A]/x \end{cases} \quad (18)$$

$$C_{B_xX_b} = \begin{cases} W_{B_xX_b}[B]/x \text{ if } [B]/x < [X]/b \\ W_{B_xX_b}[X]/b \text{ if } [X]/b < [B]/x \end{cases} \quad (19)$$

$$C_{A_yY_a} = \begin{cases} W_{A_yY_a}[A]/y \text{ if } [A]/y < [Y]/a \\ W_{A_yY_a}[Y]/a \text{ if } [Y]/a < [A]/y \end{cases} \quad (20)$$

$$C_{B_yY_b} = \begin{cases} W_{B_yY_b}[B]/y \text{ if } [B]/y < [Y]/b \\ W_{B_yY_b}[Y]/y \text{ if } [Y]/b < [B]/y, \end{cases} \quad (21)$$

where the molecular weight of the respective salt (W) is used to calculate the concentration of the salts in kg salt per kg solvent. The preceding formulas reflect the fact that the concentration of a salt is determined by the amount of the limiting counterion. The concentration of A_xX_a is at its solubility limit because point ***a*** lies on the A_xX_a saturation surface.

Solubilities and concentrations with complex-ionic equilibrium

The phase diagram for a system undergoing complex-ionic equilibrium can be calculated exactly as described in the previous sections because r_B and r_Y depend on only $[B]/z$ and $[Y]/z$, respectively. The positions of the troughs do not change on the Jänecke projection; however, the concentrations of the salts do change.

To calculate the concentrations of the salts the concentrations of the complexes must be included in the material and charge balances. Since expressions for a general system are cumbersome, the following example is used to illustrate the procedure:

$$\frac{1}{2}A_2X + \frac{1}{2}BY_2 = AY + \frac{1}{2}BX. \quad (22)$$

Table 1 shows the relationships that hold for the system. Dissociation constants for many inorganic systems are given by Linke and Seidell (1958). Solving for $[B]$ and $[Y]$ in Eqs. 2 and 3, respectively, gives

$$[B] = \frac{2r_B[A]}{(1-r_B)} \quad (23)$$

$$[Y] = \frac{r_Y[X]}{2(1-r_Y)}. \quad (24)$$

A charge balance accounts for all the species present in solution

$$[A]+[BY]+2[B] = [AX]+2[X]+[Y]. \quad (25)$$

Table 1. Dissociation Constants for Species in Eq. 22

$A_2X = AX^- + A^+$	$K_1 = \dfrac{[AX^-][A^+]}{[A_2X]}$
$AX^- = A^+ + X^{2-}$	$K_2 = \dfrac{[A^+][X^{2-}]}{[AX^-]}$
$BY_2 = BY^+ + Y^-$	$K_3 = \dfrac{[BY^+][Y^-]}{[BY_2]}$
$BY^+ = B^{2+} + Y^-$	$K_4 = \dfrac{[B^{2+}][Y^-]}{[BY^+]}$
$AY = A^+ + Y^-$	$K_5 = \dfrac{[A^+][Y^-]}{[AY]}$
$BX = B^{2+} + X^{2-}$	$K_6 = \dfrac{[B^{2+}][X^{2-}]}{[BX]}$

Again, we assume that the point on the Jänecke projection at which the concentrations are being calculated lies on the $AX_{1/2}$ saturation field. By substituting Eqs. 4, 23, 24, and the appropriate relationships given in Table 1 into Eq. 25, the following expression is obtained:

$$\frac{K_{AX_{1/2}}}{\gamma^{3/2}_{AX_{1/2}}[X]^{1/2}}\left\{1+\frac{4r_B}{(1-r_B)}+\left(\frac{r_Br_Y}{(1-r_B)(1-r_Y)K_4}-\frac{1}{K_2}\right)[X]\right\} = 2[X]+\frac{r_Y[X]}{2(1-r_Y)}. \quad (26)$$

Equation 26 involves a single unknown $[X]$, which must be calculated iteratively. It is for this reason that we do not calculate z as is done in the previous section. Once $[X]$ has been calculated, Eqs. 4, 23, and 24 as well as the dissociation constants given in Table 1 can be used to solve for the concentration of all species in solution. The solubility of A_2X is

$$S_{A_xX_a} = \begin{cases} W_{A_2X}[A]_t/2 \text{ if } [A]/2 < [X] \\ W_{A_2X}[X]_t \text{ if } [X] < [A]/2 \end{cases} \quad (27)$$

where

$$[A]_t = [A]+[AX]+2[A_2X]+[AY]$$

and

$$[X]_t = [X]+[AX]+[BX]+[A_2X]. \quad (28)$$

Equation 28 is a component mass balance on A and X.

Classification of phase behavior

We classify the phase behavior of quaternary conjugate salt systems by the location of the triple-saturation points. Figure 4 shows part of the Jänecke projection divided by the compatible salt-pair diagonal. The vertices of the hypotenuse of the triangle thus formed represent compositions of one equivalent of one of the compatible salts, $B_{1/b}Y_{1/y}$, and $A_{1/a}X_{1/x}$. The remaining vertex represents $B_{1/b}X_{1/x}$ or $A_{1/a}Y_{1/y}$, depending on whether the triangle represents the upper or the lower compositional triangle of the projection, respectively. The points α, β, χ represent the triple saturation points at three consecutive temperatures T_i, T_j, and T_k. Type I is a phase diagram in which the composition expressed in terms of $A_{1/a}X_{1/x}$ decreases, but the composition expressed in terms of $B_{1/b}Y_{1/y}$ increases as a result of moving from α to β, to χ (Figure 4a). Type II describes phase behavior in which the composition of both salts decreases as a result of moving from α toward χ (Figure 4b).

Separations from Systems of Simple Salts

Separations from systems of simple salts are grouped into three classes based on the salts recovered and on the flowsheet structures. Class I separates the compatible salts. Class II separates the incompatible salts or the two incompatible salts plus one compatible salt. Class III separates the two compatible salts plus one incompatible salt. Without loss of generality, the following discussion is in terms of monovalent salts. Since the effect of supersaturation is not considered, the designs are appropriate for both crystallization and precipitation processes. Furthermore, the processes are equally applicable to either batch or continuous operation.

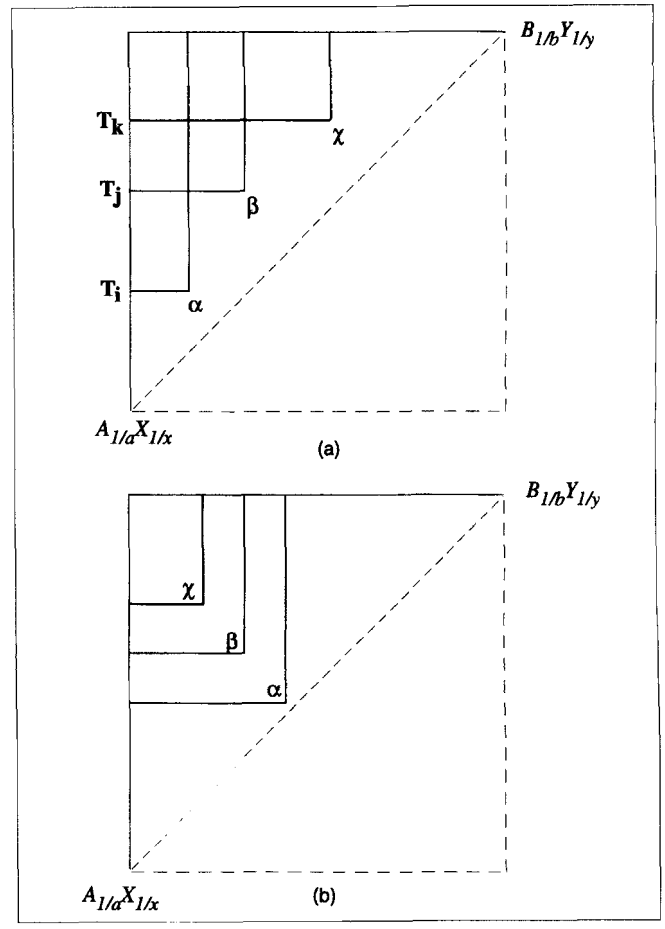

Figure 4. Classification of phase behavior based on relative compostions of the triple-saturation points α, β, and χ.

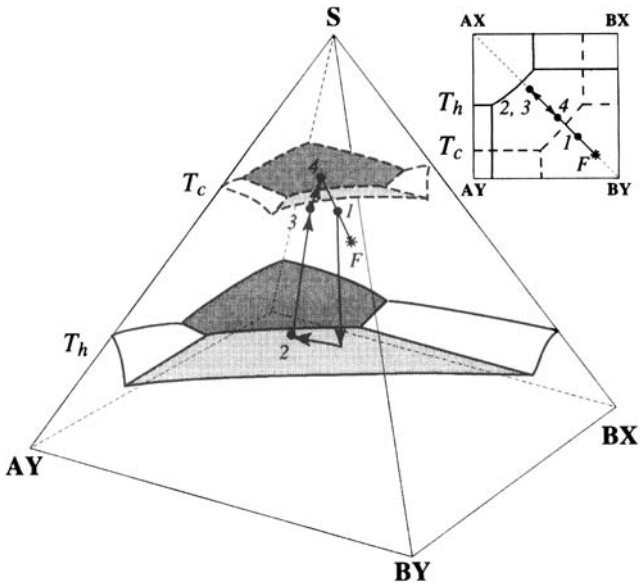

Figure 5a. Class I separation on a square-pyramid phase diagram and Jänecke projection.

Process paths are drawn for a liquid feed.

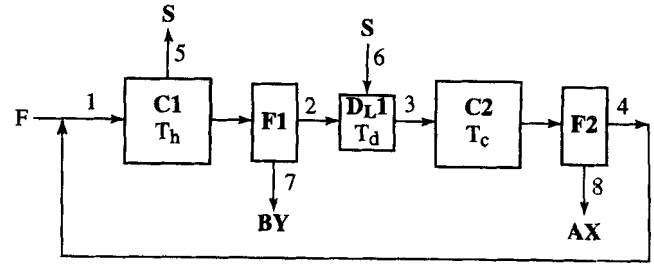

Figure 5c. Equipment configuration for Class I process paths drawn in Figure 5a.

Description of Class I separations

Class I describes any separation in which the two compatible salts are separated. It may be used only when the feed lies on the compatible-salt diagonal. The system may have either Type I or II phase behavior as long as the compatible-salt troughs at each crystallizer temperature do not intersect at the compatible-salt diagonal.

There are two cases to consider when designing a Class I process. One case involves a separation whose process path moves along the stable salt-pair diagonal while it does not in the other case. Figure 5a shows such a process for the former case on a square-pyramid phase diagram and on a Jänecke projection. Since process points (pp) 1 through 4 are collinear on the projection, the separation can also be drawn on a cross section of the phase diagram taken along the stable salt-pair diagonal (Figure 5b). Figure 5c is the flow sheet for the process. Numbered points on the phase diagram, projection, and cut correspond to the compositions of the streams in the flow sheet.

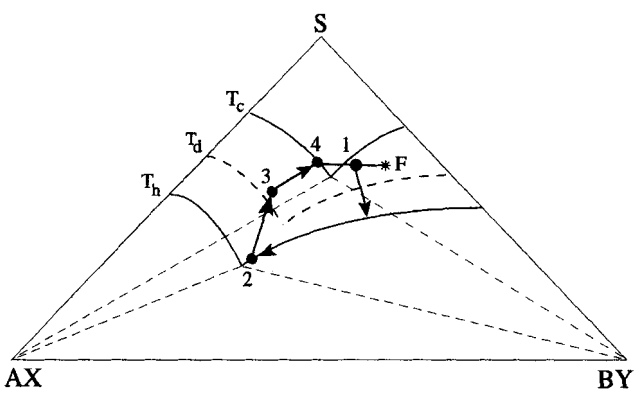

Figure 5b. Cross section of the square-pyramid phase diagram taken along the compatible-salt diagonal.

The process paths require a dilution tank between points 2 and 4 to avoid coprecipitation.

The feed for the process can be prepared in different ways. One is by dissolving a mixture of the compatible salts. Another is by dissolving a mixture of the compatible salts and incompatible salts. Yet another is by dissolving two incompatible salts. The last two possibilities rely on an equilibrium reaction to convert the incompatible salts to the compatible salts. Reacting two incompatible salts is the basis for many reactive crystallization processes. For example, silver chloride may be obtained by the following reaction in water at room temperature and ambient pressure:

$$AgNO_3 + KCl = AgCl\downarrow + KNO_3. \qquad (29)$$

Class I proceeds as follows. The feed, F, and the recycle, stream 4, are combined in a mixing tank not shown on the flow sheet to make stream 1. The tank operates at a temperature that is chosen so that stream 1 remains unsaturated. The stream is fed to the first crystallizer, $C1$, which operates at an elevated temperature, T_h. Solvent removal in $C1$ results in the selective precipitation of BY. The solid is filtered from the system. As a result of the isothermal evaporation in the crystallizer, the composition of the system moves from pp-1 to pp-2. To provide a safety margin for avoiding coprecipitation, pp-2 is located within the BY saturation field away from the T_h compatible-salt trough. The crystallizer effluent is then diluted until the composition of the solution reaches pp-3. The temperature of the dilution tank, T_d, lies between T_h and the temperature of the second crystallizer, T_c. As shown in Figure 5b, T_d is chosen so that stream 3 remains unsaturated in order to provide a safety margin from precipitation due to temperature and composition fluctuations within the tank. Naturally, T_d could be chosen to be T_h; however, this would consume more energy. The solution is then cooled to T_c in the second crystallizer, $C2$, to precipitate AX. The composition of the solution moves from pp-3 to pp-4. The composition of pp-4 lies in the AX saturation field off the T_c compatible-salt trough. The crystallizer effluent is combined with fresh feed to begin the cycle anew.

Class I design equations

The mass flow rates of solvent from $C1$ and $C2$, $F(2)$ and $F(4)$, respectively, can be calculated from the following material balances:

$$S_{BY}(T_h,2)F(2) = C_{BY}(T_c,4)F(4) \tag{30}$$

$$C_{AX}(T_h,2)F(2) = S_{AX}(T_c,4)F(4) + M_{AX}, \tag{31}$$

where M_{AX} is the mass flow rate of AX recovered from the second filter, $F2$. Solution of Eqs. 30 and 31 gives

$$F(4) = \frac{M_{AX}}{C_{AX}(T_h,2)\left\{\dfrac{C_{BY}(T_c,4)}{S_{BY}(T_h,2)} - \dfrac{S_{AX}(T_c,4)}{C_{AX}(T_h,2)}\right\}} \tag{32}$$

$$F(2) = \frac{C_{BY}(T_c,4)}{S_{BY}(T_h,2)}F(4). \tag{33}$$

In all the separation schemes presented in this article, the operating temperatures of the crystallizers and of the tanks as well as the composition of the streams immediately after dilution tanks are design variables. To illustrate this fact recall the process paths drawn on the cross-sectional cut of the phase diagram in Figure 5b. Clearly, by specifying the composition of pp-3, the compositions at pp-2 and pp-4 are set.

The composition of pp-3 strongly influences the effluent flow from $C2$. Figure 6 shows the results of fixing pp-4 while moving pp-3 along the line connecting AX and pp-4. The flow has been normalized with the value of $F(4)$ calculated when pp-2 lies at the double-saturation point at T_h. The concentration of AX has been normalized by the solubility of AX at the same point. As pp-3 moves toward pp-4, pp-2 moves away from the compatible-salt trough along the BY saturation surface, causing the concentration of AX to decrease. The lowest flows are obtained when pp-2 lies on the compatible-salt trough. As pp-3 approaches pp-4, the flow monotonically increases to infinity.

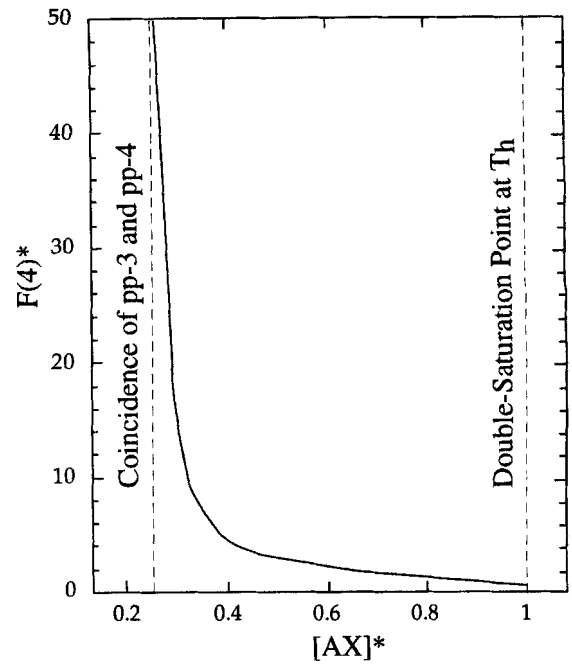

Figure 6. Recycled solvent flow rate as a function of the concentration of *AX*.

Both normalized by the respective values at the double-saturation point at T_h.

Removal of BY at the second filter

The salts may also be removed in reverse order. Figure 7 shows the process paths as well as the equipment configuration to remove AX at the first crystallizer. There are two major differences between this separation and the one presented earlier. First, the temperatures of $C1$ and $C2$ are T_c and T_h, respectively. This is the reverse of the order required to separate BY first. Second, the feed is diluted in a dilution tank (D_L1) before it is combined with the recycle.

Process economics of separation sequence

The separation sequence can strongly influence process economics. We compare the total annual cost (TAC) for separating AX first to the cost of separating BY first by calculating the capital costs for the crystallizers and heat exchangers as well as the operating cost due to steam. The cost models can be found in Peters and Timmerhaus (1980) and are not discussed in this article. A capital charge factor of one-third year is used to annualize capital costs. Filter, dryer, and preheater costs are not included because these costs are usually minor (Rajagopal et al., 1988). The most economical sequence is a strong function of salt solubilities, crystallizer temperatures, and feed composition. For the input parameters of the four cases given in Table 2, Figure 8 shows when it is more economical to separate AX first. When the solubility products are small (Case A), steam requirements dominate the cost. Increasing the values of the solubility products decreases the evaporation load and thus the steam requirements. For large solubility products (Case D), the annual capital costs dominate and the separation sequence does not

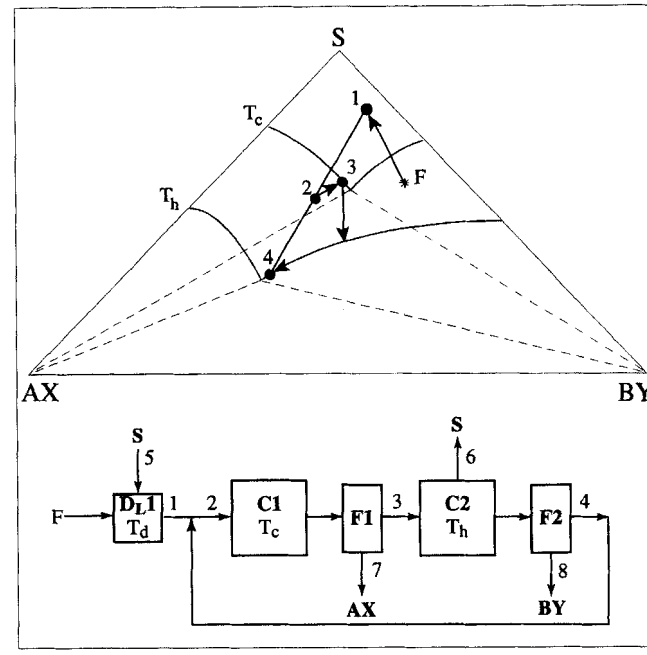

Figure 7. Process paths to remove *BY* at the second filter.

Table 2. Input Parameters for Case Studies in Figure 8

Case	A	B	C	D
K_{AX} (59°C)	1×10^{-2}	1×10^{-1}	1×10^{0}	1×10^{1}
K_{AX} (77°C)	6×10^{-2}	6×10^{-1}	6×10^{0}	6×10^{1}
K_{BY} (59°C)	2×10^{-2}	2×10^{-1}	2×10^{0}	2×10^{1}
K_{BY} (77°C)	3×10^{-2}	3×10^{-1}	3×10^{0}	3×10^{1}
Heat of vaporization of solvent			2,402 kJ/kg	
Heat of crystallization of *AX*			242 kJ/kg	
Heat of crystallization of *BY*			256 kJ/kg	
Heat capacity of solvent			4.22 kJ/kg·K	
Heat of vaporization of steam (100°C)			2,256 kJ/kg	
Total feed flow rate of salts			3,884 kg/h	
Temperature of cooling water			32°C	
ΔT cooling water			17°C	
Cost of steam			\$4.41/1,000 kg	
Cost of water			\$0.02/1,000 kg	
W			1.0 kg/mol	

affect process economics. Also notice that as the magnitude of the solubility products increases, the value of f_b at which the crossover occurs decreases.

Several heuristics have been proposed to guide selection of the separation sequence, such as separate the most plentiful first and separate the most soluble first. However, both criteria have potential pitfalls and may lead to conflicting recommendations (Ng, 1991). For this reason, it is better to directly compare the cost of the two separation sequences.

Use of a circulating salt

A circulating salt shifts the process paths off the compatible salt-pair diagonal. It is used to effect separations from systems with incongruent triple-saturation points. For example, Figure 9a shows the process paths to recover *BY* before *AX*, for which *AY* is a circulating salt. Notice that process

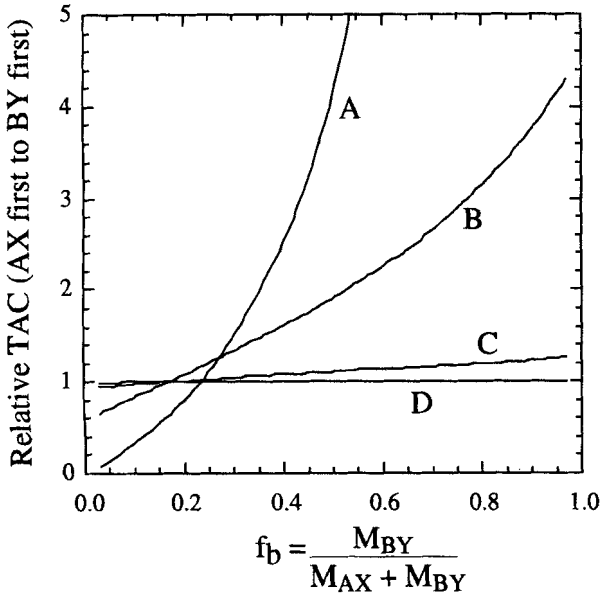

Figure 8. Comparison of the total annual cost for removing *AX* at the first filter relative to the cost for removing *BY* at the first filter.

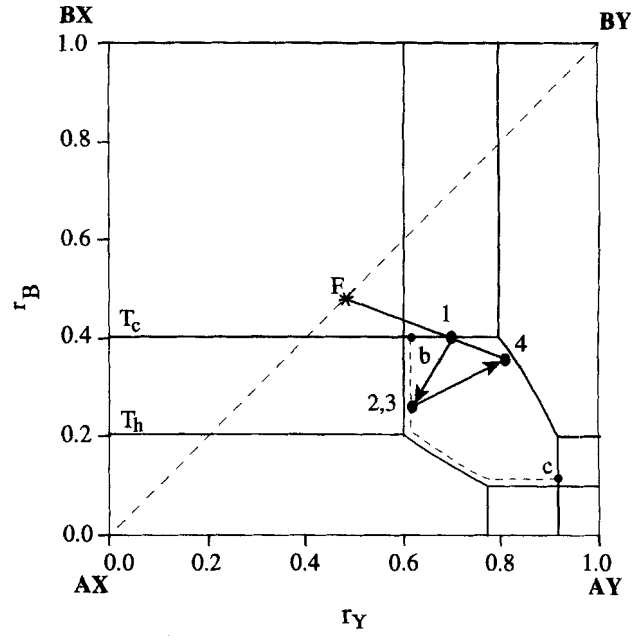

Figure 9a. Phase behavior that requires the addition of a circulating salt to recover *BY* and *AX*.

The values of the solubility products are $K_{BY}(T_h) = 1.13\times10^{-3}$, $K_{BY}(T_c) = 8\times10^{-3}$, $K_{AX}(T_h) = 3\times10^{-3}$, $K_{AX}(T_c) = 3\times10^{-3}$, $K_{BX}(T_h) = 7.51\times10^{-4}$, $K_{BX}(T_c) = 2\times10^{-3}$, $K_{AY}(T_h) = 1.03\times10^{-2}$, $K_{AY}(T_c) = 3.18\times10^{-2}$; the ratio of the mass flow rate of *BY* to *AX* is unity.

points lie in the *BY-AX-AY* composition triangle. This indicates that there is an excess of *A* and *Y* ions in the system. One way to create this excess is to add *AY* to the system during plant startup in addition to the fresh feed; however, before *AY* accumulates to a concentration where the salt precipitates, addition of this salt was stopped.

The amount of *AY* added during startup determines how far pp-3 is moved off the compatible salt-pair diagonal. The composition of pp-3 strongly affects the effluent flows from both *C*1 and *C*2. As in the separations just described, pp-2 and pp-4 should be located near double-saturation troughs to reduce the effluent flows from the crystallizer. Figure 9b plots the relative effluent solvent flow rate from *C*2, *F*(4), as the composition of pp-3 moves from point ***b*** to point ***c*** on the projection along the dotted line that tracks the double-saturation trough but without touching it. The flow rate decreases from infinity, passes through a minimum, and then approaches infinity. The solvent flow and concentration of *AY* are normalized to their respective values at $r_B = 0.2$ and $r_Y = 0.6$, which correspond to a minimum in *F*(4). Notice that the amount of circulating salt that minimizes the flow corresponds to the point where pp-3 lies near a triple-saturation point at T_h. Clearly, addition of a circulating salt strongly affects process economics. It should be considered only for systems with incongruently saturated triple-saturation points.

Class II separations

The incompatible salts are recovered by Class II separations. Process point 1 must lie in the saturation field of the incompatible salt to be removed at *F*(1). When the system

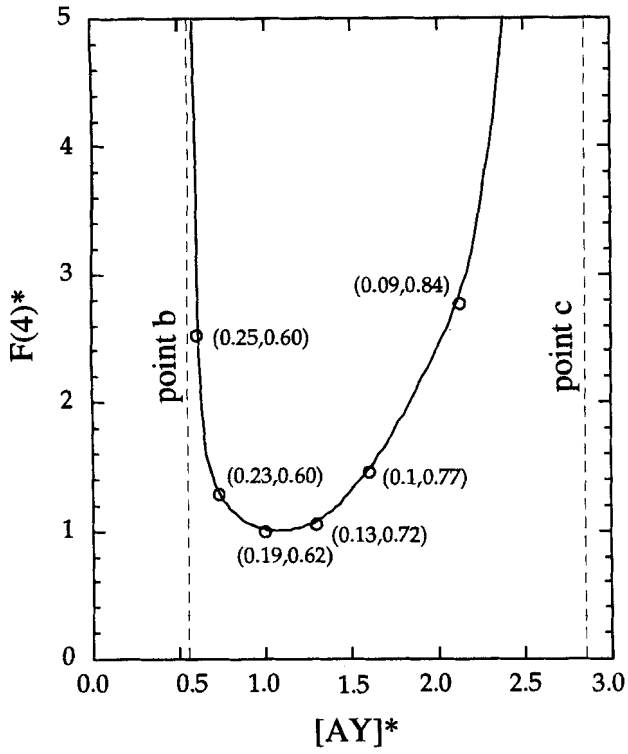

Figure 9b. Recycled solvent flow rate as a function of the amount of circulating salt *AY* added to the system.

Both are normalized by the respective values at the point with the lowest recycle flow rate.

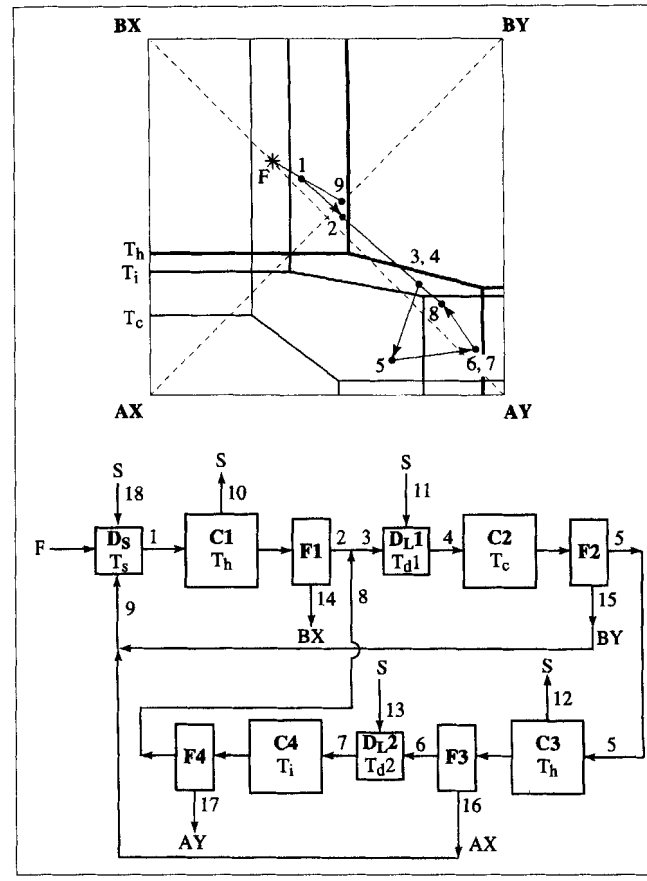

Figure 10. Process paths and equipment configuration for Class IIA.

exhibits Type I phase behavior in the lower compositional triangle, three isotherms are required to effect the separation. Figure 10 shows the process paths and equipment configuration for such a case (Class IIA), which recovers *BX* at *F*1 and *AY* at *F*4. The feed must lie on the incompatible salt-pair diagonal. Notice that the solid recycle streams 15 and 16 are combined to make stream 9. Streams 9, 18, and the feed are combined in a dissolution tank held at T_s so that stream 1 is saturated with *BX*. The process points that are design variables are pp-1, pp-4, and pp-7.

The flow rates may be calculated from the following design equations:

$$C_{AY}(T_h,6)F(6) = S_{AY}(T_i,8)F(8) + M_{AY} \quad (34)$$

$$S_{AX}(T_h,6)F(6) = C_{AX}(T_i,8)F(8) \quad (35)$$

$$S_{BY}(T_c,5)F(5) = C_{BY}(T_h,6)F(6) \quad (36)$$

$$S_{BX}(T_s,1)F(1) = S_{BX}(T_h,2)F(2) + M_{BX} \quad (37)$$

$$C_{AY}(T_s,1)F(1) = C_{AY}(T_h,2)F(2). \quad (38)$$

The mass balances are written so that only solid flows M_{AY} and M_{BX} appear in the equations. The solution to these equations is straightforward and is not presented here. Since all solids other than *AY* and *BX* are recycled, the value of M_{AY} equals the flow of *A* and *Y* in the feed. Likewise, M_{BX} equals the amount of *B* and *X* in the feed.

The choice of the composition of the process-point design variables is very important. Process point 1 is determined by a trade-off between dissolver size and evaporation load at *C*1. Process point 2 should be as close to a double-saturation trough as safety margin permits. The composition at pp-4 sets the bounds for the possible values for pp-7, which is also a design variable. It is advisable to choose pp-4 so that pp-7 lies well within the *AY* saturation field at T_i in order to maximize the recovery of *AY*.

When the feed does not lie on the incompatible salt-pair diagonal, the incompatible salts plus one compatible salt are obtained. For example, Class IIA can be used to obtain the incompatible pair along with *BY* when the feed lies in the *BX-BY-AY* compositional triangle. The only flow sheet modification is that stream 15 is not recycled (Figure 10).

Figure 11 shows the process paths and equipment configuration for separating the incompatible salts when the system exhibits Type II phase behavior in the lower compositional triangle. Class IIB requires only two isotherms, and process points 3 and 5 are design variables. Process point 1 is fixed by assuming that stream 1 is saturated with *BX*. Even though the curvature of the T_h compatible-salt trough is exaggerated for clarity, the separation does not rely on this feature.

Class III separations

Class III separations are used to obtain the two compatible salts plus one incompatible salt. The feed must not lie on either the compatible or the incompatible salt-pair diagonal.

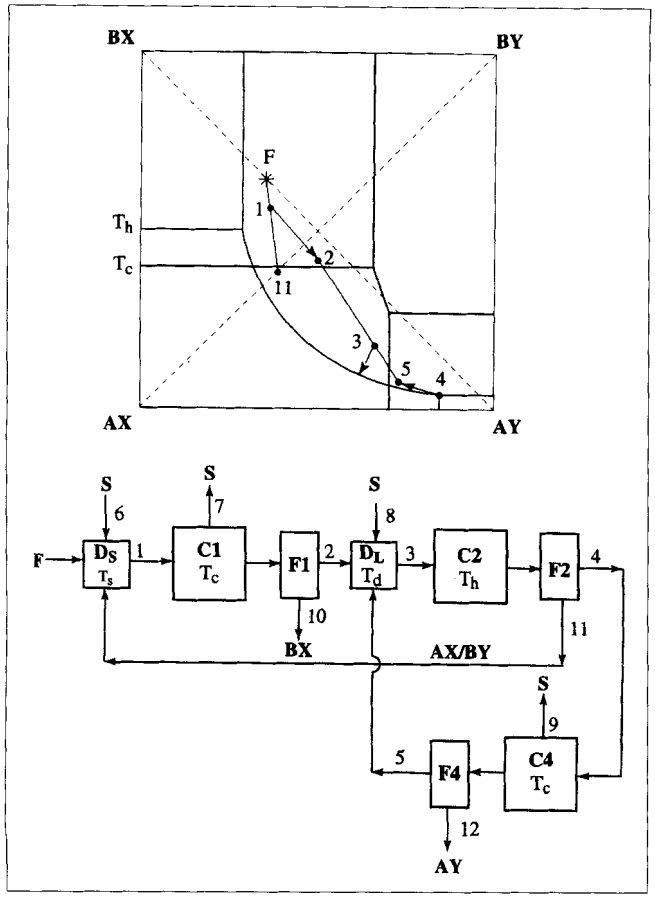

Figure 11. Process paths and equipment configuration for Class IIB.

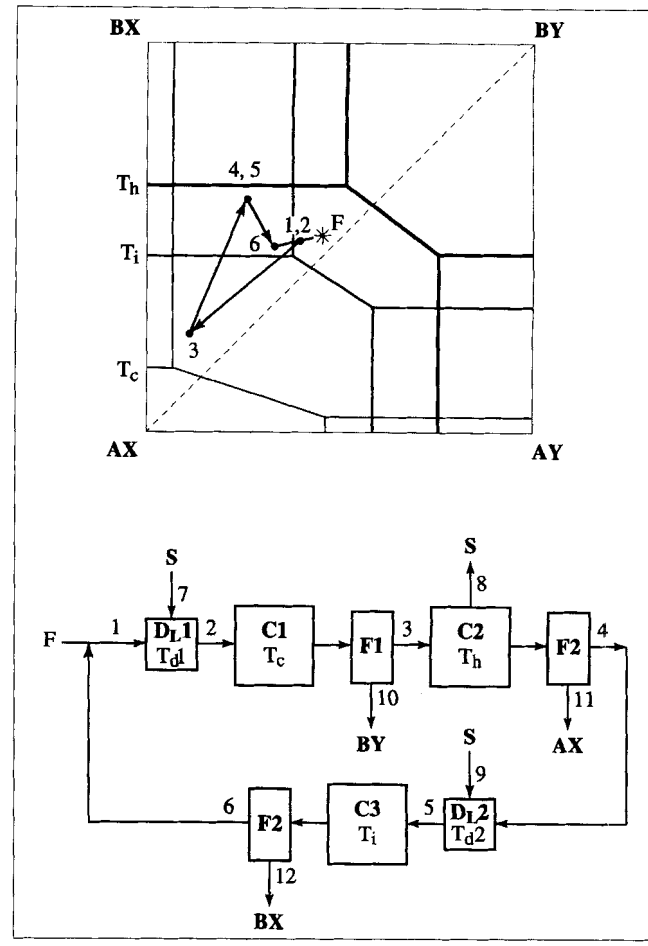

Figure 12. Process paths and equipment configuration for Class IIIA.

The product salts belong to the same compositional triangle as the feed. There are three types of process paths that obtain the desired products. The three schemes are classified by the phase behavior in the compositional triangle in which the process paths are drawn.

Class IIIA utilizes differences in solubility of the three salts at three different temperatures, T_c, T_i, T_h. The phase behavior must be Type I in the upper compositional triangle. The triple-saturation points may be either congruently or incongruently saturated in the compositional triangle of the product salts. It is desirable for the triple saturation points in the other compositional triangle to be congruently saturated. Figure 12 shows the process paths for separating *BY*, *AX*, and *BX* sequentially. *BY* can be removed at T_c, *AX* can be removed at T_h, and *BX* can be removed at T_i. Process points 2 and 5 are design variables.

Figure 13 shows the use of Class IIIB to separate *BY*, *BX*, and *AX* sequentially. Like Class IIIA, Class IIIB uses three temperatures; however, the process requires Type II phase behavior in the upper compositional triangle. As in Class IIIA, there are no restrictions on the triple-saturation points. Class IIIB removes *BY* at T_i, *BX* at T_c, and *AX* at T_h. The process-point design variables are pp-3 and pp-5.

Class IIIC requires only two temperatures and removes the incompatible salt first, and then the two compatible salts. It may operate with either Type I or II phase behavior. Furthermore, pp-1 must lie in the saturation field of the incompatible salt. Figure 14 gives the process paths to separate *BX*, *BY*, and then *AX*. Process points 3 and 5 are design variables.

Design equations for Class III

Design equations for Class III separations can be developed as before. For example, we have for Class IIIA

$$S_{BY}(T_c,3)F(3) = C_{BY}(T_h,4)F(4) \tag{39}$$

$$C_{AX}(T_c,3)F(3) = S_{AX}(T_h,4)F(4) + M_{AX} \tag{40}$$

$$C_{BX}(T_h,4)F(4) = S_{BX}(T_i,6)F(6) + M_{BX}. \tag{41}$$

Process point 2 is the most important process-point design variable in this scheme because it determines the bounds for the composition of pp-5. Therefore, pp-2 should be chosen so that pp-5 can be placed well within the *BX* saturation field.

Separations from Systems with Compounds and Hydrates

In many systems the presence of hydrates and compounds complicates the separation of the pure salts. It is no longer

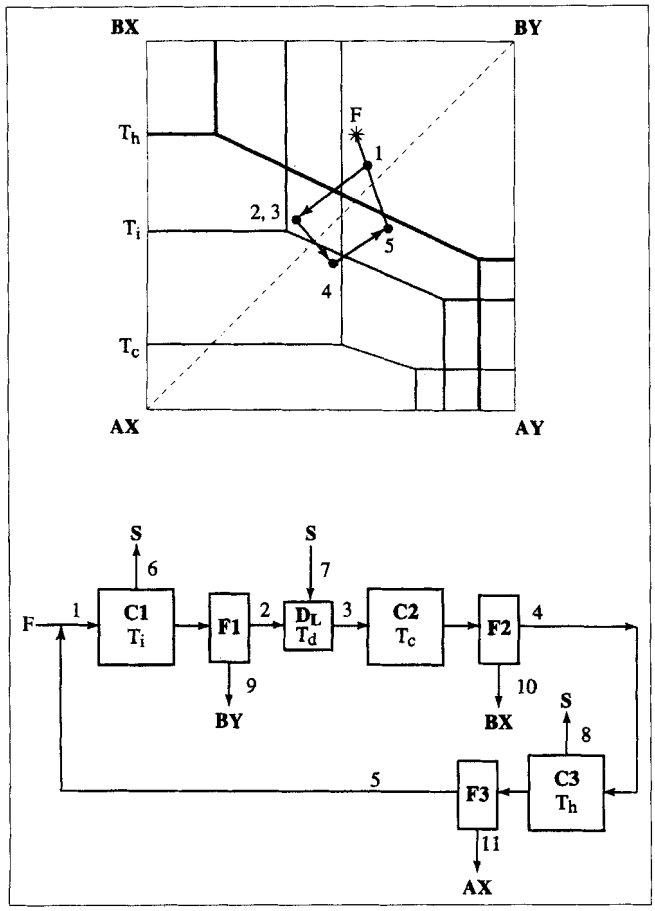

Figure 13. Process paths and equipment configuration for Class IIIB.

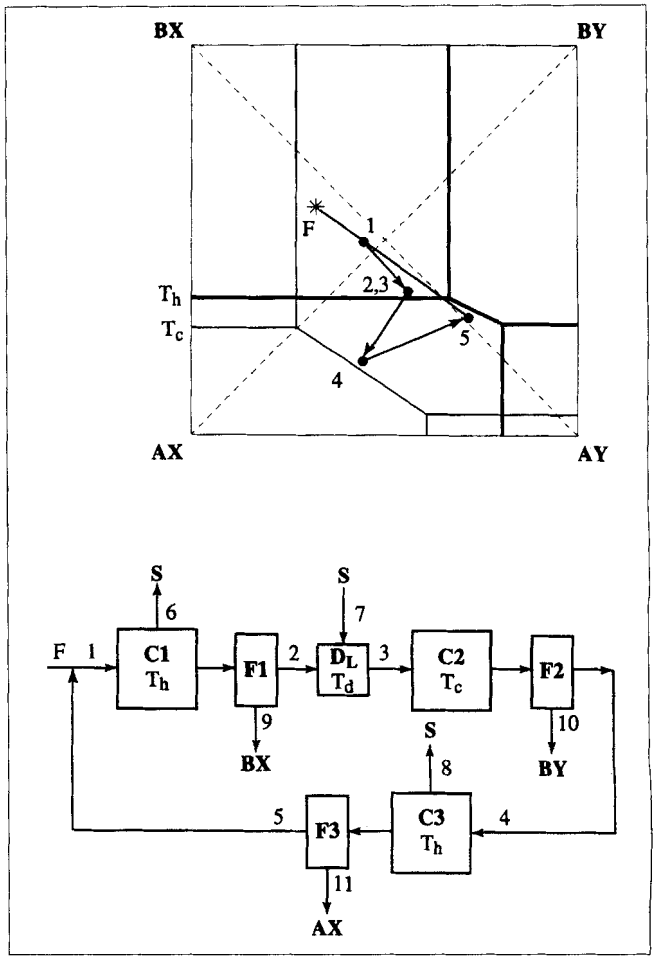

Figure 14. Process paths and equipment configuration for Class IIIC.

possible to calculate the phase diagram as previously described; however, an iterative method using solubility products is available (Kusik et al., 1979). Due to the complex phase behavior of these systems, each separation must be considered on a case by case basis. Furthermore, the composition of the feed also dictates the feasibility of a separation via fractional crystallization. Like Classes I through III, the success of a separation with hydrates and compounds relies on utilizing overlapping saturation fields at different temperatures as well as on combining streams to move around the phase diagram. To illustrate how to synthesize such a separation, consider the process paths and the equipment configuration for a system from which *AX*, *BY*, *AY*, *BX*, *AY*·3*BY*, *AY*·H_2O, and *AY*·*AX*·H_2O may precipitate. The desired products are assumed to be *AX* and *BY*. The projection at T_c is a sketch of a system consisting of KNO_3, K_2SO_4, Na_2SO_4, $NaNO_3$, and water at 30°C (Purdon and Slater, 1946). The T_h isotherm is a sketch of the same system with the troughs shifted.

In Figure 15 the feed at T_h lies in the *BY* saturation field. Dropping the temperature to T_c and removing solvent causes *BY* to precipitate until the system reaches a composition given by pp-1. Process point 2 is formed by combining the crystallizer effluent, stream 1, with the recycle stream given by pp-7. The dilution tank temperature, T_d, is between T_c and T_h. Af-

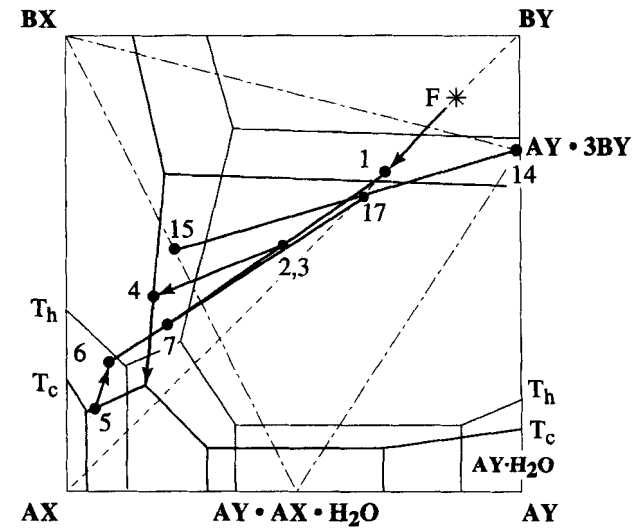

Figure 15a. Process paths for obtaining *AX* and *BY* from a system that can form compounds and hydrates.

The feed lies over the *BY* saturation field.

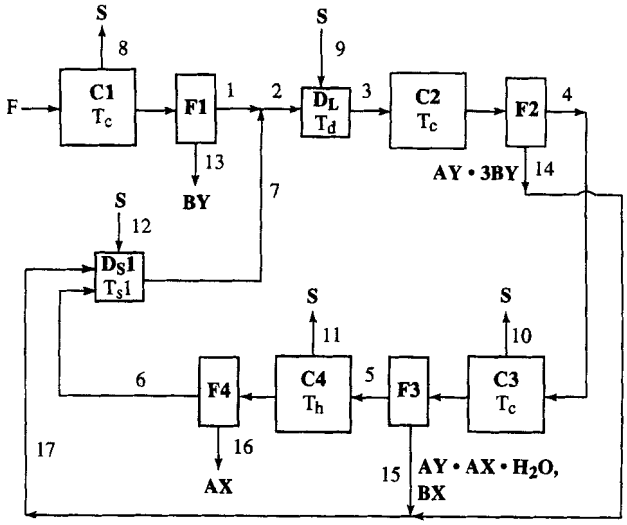

Figure 15b. Equipment configuration for process paths given in Figure 15a.

ter adjusting solvent, $AY{\cdot}3BY$ precipitates upon cooling. The crystallizer mother liquor is sent to $C3$, where a mixture of $AY{\cdot}AX{\cdot}H_2O$ and BX precipitates. The solids recovered by $F3$, stream 15, are combined with those recovered by $F2$, stream 14, to make stream 17. The composition of the mother liquor from $C3$ is given by pp-5. Even though $C2$ and $C3$ operate at T_c, it is not possible to move directly from pp-3 to pp-5 in one crystallization step. This is because pp-4 must lie in the $BX/AY{\cdot}AX{\cdot}H_2O/AX$ compositional triangle. Solvent is removed from stream 5 in $C4$, which operates at T_h. AX is filtered from the process. The crystallizer effluent, stream 6, is combined with fresh solvent and stream 17 in a dissolver. Stream 7 is unsaturated.

Conclusions

A method for the conceptual design of fractional crystallization separation processes is presented. It is applicable to separate minerals and optical isomers from conjugate salt solutions. Furthermore, the method can be used to predict the products of reactive crystallization processes. The method includes a procedure to calculate the phase diagram and Jänecke projection. Equations required to calculate the concentrations of all the species in solution are also derived. Three general classes of separations are proposed to separate simple salts from solution. The classes are based on phase behavior and the composition of the feed. The operating temperatures of the crystallizers and of the tanks as well as the composition of process streams immediately after dilution tanks are design variables. It is also shown that the basic operations used in fractional crystallization can be used to recover simple salts from systems from which compounds and hydrates may precipitate.

The choice of solvent should be based on three criteria. The solubility product should determine the salt solubility. The salts should have a high solubility in the solvent. This results in reduced heating, cooling, solvent evaporation, and solvent addition. The solvent should be chosen so that the composition of the double-saturation troughs at different operating temperatures are apart from one another on the phase diagram. For example, the farther apart the BY/AX double-saturation troughs at T_h and T_c, the lower the flows (Figure 5a).

The current design method can be improved in three areas. First, many industrial crystallization processes do not attain equilibrium; therefore, dynamic phase diagrams should be used in place of equilibrium diagrams (Hadzeriga, 1967). Calculation of concentrations of the species in solution from dynamic phase diagrams is not possible by the method presented in this article, however. Second, because the method relies on drawing process paths directly on a Jänecke projection, the extension of the method to higher dimensional systems is unclear. Third, more heuristics need to be developed to expedite the determination of the most economical separation sequence.

Acknowledgment

The support of the National Science Foundation (Grant CTS-9220196) for this research is gratefully acknowledged.

Notation

C_{IJ} = concentration of salt IJ (kg salt/kg solvent)
D_S = dissolution tank
f_b = mass fraction of BY in a mixture of BY and AX
$F(k)$ = mass flow rate of solvent in stream k (kg/h)
$[IJ]$ = concentration of salt IJ (molality)
K = dissociation constant
S = makeup solvent
S_{IJ} = solubility of salt IJ (kg salt/kg solvent)
W_{IJ} = molecular weight of salt IJ

Greek letter

γ = activity coefficient

Subscripts

s = dissolver
t = total

Literature Cited

Ainsworth, S. J., "Soaps and Detergents," *Chem. Eng. News*, 34, Jan. 24 (1994).
Butler, J. N, *Ionic Equilibrium*, Addison-Wesley, Reading, MA (1964).
Cisternas, L. A., and D. F. Rudd, "Process Designs for Fractional Crystallization from Solution," *Ind. Eng. Chem. Res.*, **32**(9), 1993 (1993).
Chang, J., "Solubility Product Constants," *Handbook of Chemistry and Physics*, 70th ed., CRC Press, Boca Raton, FL (1990).
Dye, S. R., and K. M. Ng, "Bypassing Eutectics with Extractive Crystallization: Design Alternatives and Tradeoffs," *AIChE J.*, **41**, 1456 (1995a).
Dye, S. R., and K. M. Ng, "Fractional Crystallization: Design Alternatives and Tradeoffs," *AIChE J.*, **41**, 2427 (1995b).
Fitch, B., "How to Design Fractional Crystallization Processes," *Ind. Eng. Chem.*, **62**(12), 6 (1970).
Fleck, G. M., *Equilibria in Solution*, Holt, Rinehart & Winston, New York (1966).
Fogassy, E., et al., "Structural Studies on Optical Resolution via Diasteroisomeric Salt Formation. Enantiomer Separation for *cis*-Permethrinic Acid [*cis*-2,2-Dimethyl-3-(2,2-dichlorovinyl)cyclopropanecarboxylic Acid]," *Chem. Soc. Perkin Trans. II*, 1385 (1988).
Fuyuhiro, A., K. Yamanari, and Y. Shimura, "Solubility Isotherms of Reciprocal Salt-Pairs of Optically Active Cobalt(III) Complexes," *Bull. Chem. Soc. Japan*, **52**(1), 90 (1979).
Hadzeriga, P., "Dynamic Equilibria in the Solar Evaporation of the Great Salt Lake Brine," *SME Trans.*, **240**, 413 (1967).

Hightower, J. V., "The Trona Process and Its Unique Features," *Chem. Eng.*, 104 (Aug., 1951).
Jongema, P., "Process of the Preparation of Sodium Chloride," U.S. Patent 5,221,528 (1993).
Kusik, C. L., H. P. Meissner, and E. L. Field, "Estimation of Phase Diagrams and Solubilities for Aqueous Multi-ion Systems," *AIChE J.*, **25**, 759 (1979).
Linke, W. F., and A. Seidell, *Solubilities, Inorganic and Metalorganic Compounds*, 4th ed., Van Nostrand, Princeton, NJ (1958).
Mehta, V. C., "Process for Recovering Lithium from Salt Brines," U.S. Patent 4,723,962 (1988).
Meissner, H. P., and C. L. Kusik, "Double Salt Solubilities," *Ind. Eng. Chem. Proc. Des. Dev.*, **18**, 391 (1979).
Meul, T., "Process for Resolution of Racemates of 2,2-dimethylcyclopropanecarboxylic Acid," U.S. Patent 5,166,417 (1992).
Mullin, J. W., *Crystallization*, 3rd ed., Butterworth-Heinemann, Oxford (1993).
Nicolaisen, H., P. Rasmussen, and J. M. Sorensen, "Correlation and Prediction of Mineral Solubilities in the Reciprocal Salt System $(Na^+, K^+)(Cl^-, SO_4^{2-})$-$H_2O$ at 0–100°C," *Chem. Eng. Sci.*, **48**(18), 3149 (1993).
Ng, K. M., "Systematic Separation of a Multicomponent Mixture of Solids Based on Selective Crystallization and Dissolution," *Separations Tech.*, **1**, 108 (1991).
Paul, E. L., and C. B. Rosas, "Challenges for Chemical Engineers in the Pharmaceutical Industry," *Chem. Eng. Prog.*, **86**(12), 17 (1990).
Peters, M. S., and K. D. Timmerhaus, *Plant Design and Economics for Chemical Engineers*, 3rd ed., McGraw-Hill, New York (1980).
Pitzer, K. S., "Thermodynamics of Electrolytes. I. Theoretical Basis and General Equations," *J. Phys. Chem.*, **77**(2), 268 (1973).
Purdon, F. F., and V. W. Slater, *Aqueous Solution and the Phase Diagram*, Arnold, London (1946).
Rajagopal, S., K. M. Ng, and J. M. Douglas, "Design of Solids Processes: Production of Potash," *Ind. Eng. Chem. Res.*, **27**, 2071 (1988).
Rajagopal, S., K. M. Ng, and J. M. Douglas, "Design and Economic Trade-Offs of Extractive Crystallization Processes," *AIChE J.*, **37**, 437 (1991).
Ricci, J. E., *The Phase Rule and Heterogeneous Equilibrium*, Van Nostrand, New York (1951).
Sohnel, O., and J. Garside, *Precipitation: Basic Principles and Industrial Applications*, Butterworth-Heinemann, Oxford (1992).
Stinson, S. C., "Chiral Drugs," *Chem. Eng. News*, 38, Sept. 19 (1994).

Manuscript received July 24, 1995, and revision received Nov. 16, 1995.